High-Latitude Forcing of the South American Summer Monsoon During the Last Glacial

Lisa C. Kanner, *et al.*

Science **335**, 570 (2012);
DOI: 10.1126/science.1213397

makes catalyst recovery challenging. We focused our experiments on the cross-linking of two commercial silicone fluids: SilForce SL6100 and SilForce SL6020 (Momentive Performance Materials, Waterford, NY) (Fig. 3). Addition of a toluene solution containing 1000 ppm of (^{iPr}PDI)Fe(N_2)$_2$ to a neat mixture of the two fluids at 23°C resulted in immediate cross-linking. Dissolving the iron compound in a small amount of toluene is necessary because of the low solubility of (^{iPr}PDI)Fe(N_2)$_2$ in the silicone fluids. We also observed immediate cross-linking upon addition of 500 ppm of [(^{Me}PDI)Fe(N_2)]$_2$(μ_2-N_2) in toluene solution. With the more active [(^{Me}PDI)Fe(N_2)]$_2$(μ_2-N_2) compound, cross-linking could be achieved over the course of 2 hours in neat silicone fluid without the addition of toluene. In each case that we studied, the resulting silicone polymer was identical to material prepared commercially using platinum catalysts. Photographs are presented in Fig. 3 for visual comparison.

Collectively, these results demonstrate the potential of Earth-abundant metal complexes to compete with more rare and more expensive precious-metal counterparts. Beyond their high activities, the iron compounds offer functional-group tolerance and, perhaps most importantly, exclusive regioselectivity that obviates the need for separation of unwanted by-products obtained in industrial processes.

References and Notes

1. B. Marciniec, J. Gulinski, W. Urbaniak, Z. W. Kornetka, in *Comprehensive Handbook on Hydrosilylation*, B. Marciniec, Ed. (Pergamon, Oxford, 2002), pp. 3–7.
2. B. Marciniec, *Coord. Chem. Rev.* **249**, 2374 (2005).
3. V. B. Pukhnarevitch, E. Lukevics, L. I. Kopylova, M. Voronkov, *Perspectives of Hydrosilylation* (Institute for Organic Synthesis, Riga, Latvia, 1992).
4. I. Ojima, in *The Chemistry of Organic Silicon Compounds*, S. Patai, Z. Rappoport, Eds. (Wiley Interscience, New York, 1989), pp. 1479–1526.
5. A. K. Roy, *Adv. Organomet. Chem.* **55**, 1 (2007).
6. A. F. Noels, A. J. Hubert, in *Industrial Applications of Homogeneous Catalysis*, A. Mortreux, Ed. (Kluwer, Amsterdam, 1985), pp. 80–91.
7. E. Plueddemann, *Silane Coupling Agents* (Plenum Press, New York, ed. 2, 1991).
8. R. M. Hill, in *Silicone Surfactants, Surfactants Science Series*, vol. 86, R. M. Hill, Ed. (Marcel Dekker, New York, 1999), pp. 1–48.
9. M. Wong, E. Memisha, U.S. Patent 6,805,856 (2004).
10. I. E. Markó *et al.*, *Science* **298**, 204 (2002).
11. O. Buisine *et al.*, *Chem. Commun.* **2005**, 3856 (2005).
12. P. B. Hitchcock, M. F. Lappert, N. J. W. Warhurst, *Angew. Chem. Int. Ed. Engl.* **30**, 438 (1991).
13. A. J. Holwell, *Platin. Met. Rev.* **52**, 243 (2008).
14. C.-J. Yang, *Energy Policy* **37**, 1805 (2009).
15. P. J. Chirik, K. Wieghardt, *Science* **327**, 794 (2010).
16. S. Enthaler, K. Junge, M. Beller, in *Iron Catalysis in Organic Chemistry*, B. Plietker, Ed. (Wiley-VCH, Weinheim, Germany, 2008), pp. 125–142.
17. W. M. Czaplik, M. Mayer, J. Cvengros, A. J. von Wangelin, *ChemSusChem* **2**, 396 (2009).
18. J. Y. Corey, J. Braddock-Wilking, *Chem. Rev.* **99**, 175 (1999).
19. M. Zhang, A. Zhang, *Appl. Organomet. Chem.* **24**, 751 (2010).
20. M. A. Schroeder, M. S. Wrighton, *J. Organomet. Chem.* **128**, 345 (1977).
21. R. D. Sanner, R. G. Austin, M. S. Wrighton, W. D. Honnick, C. U. Pittman, *Inorg. Chem.* **18**, 928 (1979).
22. R. H. Morris, *Chem. Soc. Rev.* **38**, 2282 (2009).
23. P. J. Chirik, in *Catalysis Without Precious Metals* (Wiley-VCH, Weinheim, Germany, 2010), pp. 83–106.
24. B. Marciniec, *Silicon Chem.* **1**, 155 (2002).
25. J. C. Mitchener, M. S. Wrighton, *J. Am. Chem. Soc.* **103**, 975 (1981).
26. F. Kakiuchi, Y. Tanaka, N. Chatani, S. Murai, *J. Organomet. Chem.* **456**, 45 (1993).
27. S. C. Bart, E. Lobkovsky, P. J. Chirik, *J. Am. Chem. Soc.* **126**, 13794 (2004).
28. J. Y. Wu, B. N. Stanzl, T. Ritter, *J. Am. Chem. Soc.* **132**, 13214 (2010).
29. S. K. Russell, J. M. Darmon, E. Lobkovsky, P. J. Chirik, *Inorg. Chem.* **49**, 2782 (2010).
30. J. W. Sprengers, M. de Greef, M. A. Duin, C. J. Elsevier, *Eur. J. Inorg. Chem.* **2003**, 3811 (2003).
31. R. J. Trovitch, E. Lobkovsky, P. J. Chirik, *J. Am. Chem. Soc.* **130**, 11631 (2008).
32. P. J. G. Stevens, *Pestic. Sci.* **38**, 103 (1993).

Acknowledgments: We thank Momentive Performance Materials for financial support. Portions of this work have been published in the following patent applications: US2011/0009573 A1 and U.S. serial no. 13/325,250.

Supporting Online Material

www.sciencemag.org/cgi/content/full/335/6068/567/DC1
SOM Text
Figs. S1 to S14
Tables S1 to S3
References (*33*, *34*)

26 September 2011; accepted 29 November 2011
10.1126/science.1214451

High-Latitude Forcing of the South American Summer Monsoon During the Last Glacial

Lisa C. Kanner,[1]* Stephen J. Burns,[1] Hai Cheng,[2,3] R. Lawrence Edwards[3]

The climate of the Last Glacial period (10,000 to 110,000 years ago) was characterized by rapid millennial-scale climate fluctuations termed Dansgaard/Oeschger (D/O) and Heinrich events. We present results from a speleothem-derived proxy of the South American summer monsoon (SASM) from 16,000 to 50,000 years ago that demonstrate the occurrence of D/O cycles and Heinrich events. This tropical Southern Hemisphere monsoon reconstruction illustrates an antiphase relationship to Northern Hemisphere monsoon intensity at the millennial scale. Our results also show an influence of Antarctic millennial-scale climate fluctuations on the SASM. This high-resolution, precisely dated, tropical precipitation record can be used to establish the timing of climate events in the high latitudes of the Northern and Southern Hemispheres.

Dansgaard/Oeschger (D/O) and Heinrich events have been recognized in many terrestrial and marine records, particularly from the Northern Hemisphere. First observed in oxygen isotope ratios of ice cores from Greenland (*1*), the D/O cycles are interpreted as large abrupt warmings (interstadials) followed by more gradual cooling to stadial conditions. The D/O cycles are particularly well expressed in tropical Northern Hemisphere speleothem records, where cold and warm periods in Greenland are coincident with dry and wet periods, respectively, in the East Asian and Indian summer monsoons (EASM and ISM) (*2*–*4*). The presence of D/O cycles in the Southern Hemisphere, or their relation to Southern Hemisphere monsoons, has not been established, however. Heinrich events are pronounced cold intervals (~500 ± 250 years in duration) marked by horizons of ice-rafted debris in ocean sediment cores from mid-latitudes in the Atlantic Ocean (*5*–*7*). Although an interhemispheric antiphased relation has been observed for the Heinrich (H1 to H6) events, the specific timing and duration are less well constrained because of uncertainties in ocean reservoir ages (*8*) and changes in sediment accumulation rates. Here we present a high-resolution, precisely dated, speleothem reconstruction of South American summer monsoon (SASM) intensity for the Last Glacial period. This record demonstrates the presence of D/O cycles in the SASM, where an intensified SASM is associated with stadial events in Greenland. In addition, we identify millennial-scale climate events that resulted from the interplay between rapid Antarctic warming and cool North Atlantic Heinrich events. Finally, we use the signature of the major D/O cycles to propose possible constraints on the timing and duration of Heinrich events H4 and H5.

We collected stalagmite P09-PH2 from Pacupahuain Cave (11.24°S, 75.82°W; 3800 m above sea level) in the central Peruvian Andes (fig. S1). Pacupahuain Cave was formed in a Triassic dolomitic limestone massif (*9*) and in an area where glacial landforms are not present. P09-PH2 is a calcite stalagmite 16 centimeters tall and was collected in the cave's main gallery about 500 m from the entrance. The speleothem was halved along the growth axis and subsampled along growth layers for radiometric dating, using uranium-thorium (U-Th) techniques by

[1]Department of Geosciences, University of Massachusetts, Amherst, MA 01002, USA. [2]Institute of Global Environmental Change, Xi'an Jiaotong University, Xi'an 710049, China. [3]Department of Geology and Geophysics, University of Minnesota, Minneapolis, MN 55455, USA.

*To whom correspondence should be addressed. E-mail: lkanner@geo.umass.edu

multicollector inductively coupled plasma mass spectroscopy (MC-ICP-MS) (*10*, *11*). Seventeen ^{230}Th dates, all in stratigraphic order, have analytical errors <0.4% (fig. S2 and table S1). An age model was developed based on linear interpolation between adjacent age measurements, yielding an age range for the sample of 16,020 to 49,470 years before the present (yr B.P., with the present = 1950).

Stable oxygen and carbon isotope ratios (δ^{18}O and δ^{13}C) were measured on 1076 micromilled samples taken along the growth axis. The average sampling resolution is approximately 30 years. The very low correlation (coefficient of determination $r^2 = 0.1$) between δ^{13}C and δ^{18}O values along the growth axis (fig. S3) indicates that kinetic fractionation did not significantly influence speleothem isotopic variability (*11*, *12*). P09-PH2 δ^{18}O values range from –14 per mil (‰) to –17.5‰ between 16 and 50 thousand yr B.P. (ky B.P.) (Fig. 1). The δ^{18}O record is characterized by high-amplitude millennial-scale events, with rapid increases of up to 2.5‰ occurring over a century or less. The decline to local δ^{18}O minima occurred more gradually, over periods ranging from a few centuries to a few millennia. The lowest values in the record occur over an extended period of time between 28.8 to 30.3 ky B.P. The highest values are attained over very brief intervals at 16, 37, 38, and 47 ky B.P.

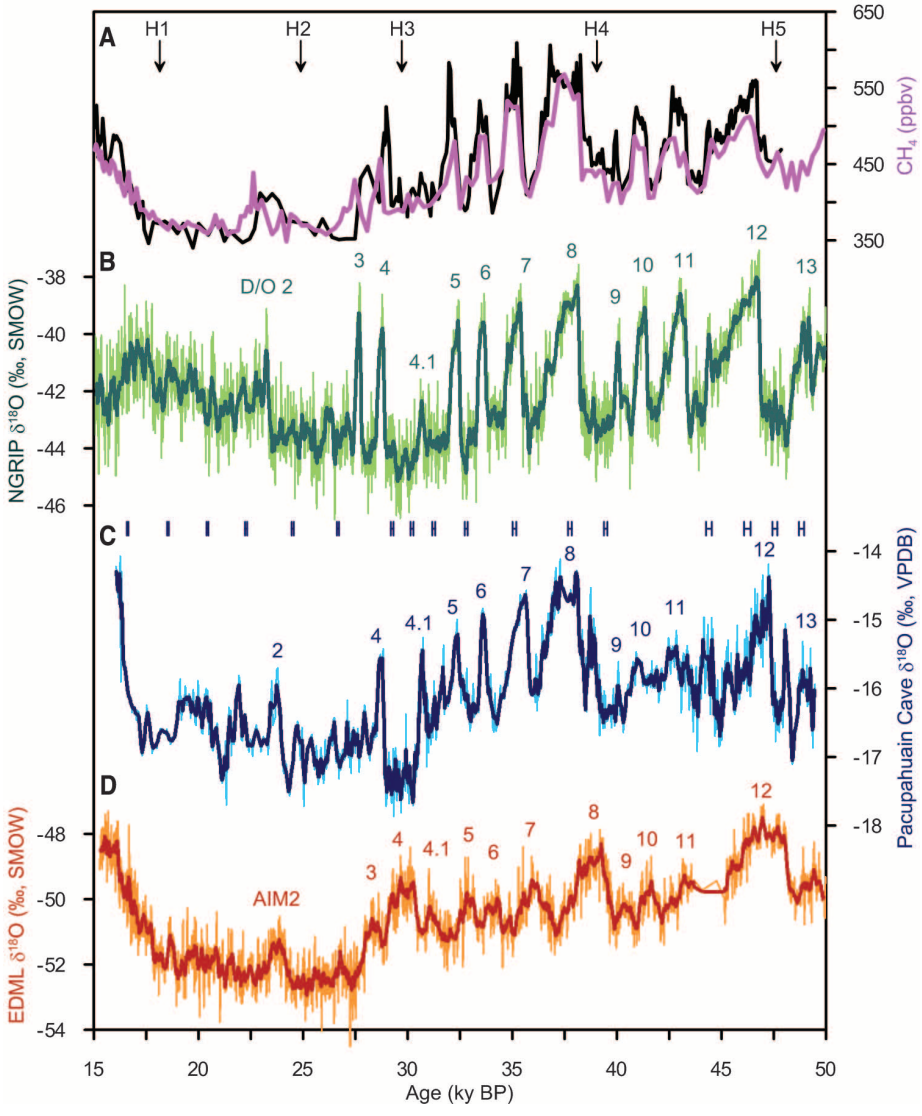

Fig. 1. The δ^{18}O reconstruction of stalagmite P09-PH2 compared to high-latitude ice core δ^{18}O and CH_4 concentrations. SMOW, standard mean ocean water standard; ppbv, parts per billion by volume; VPDB, Vienna Pee Dee belemnite standard. (**A**) GRIP and NGRIP CH_4 (black) (*24*, *25*) and EDML CH_4 (purple) (*23*) concentrations. (**B**) NGRIP ice core δ^{18}O (dark green, 7-point running mean) (*22*). (**C**) Speleothem P09-PH2 δ^{18}O time series with U/Th dates with 2σ uncertainty bars (dark blue, 3-point running mean). (**D**) EDML ice core δ^{18}O (red, 7-point running mean) (*23*). The age models for Greenland and Antarctica δ^{18}O and NGRIP and EDML CH_4 concentrations from (*22*) are shown. GRIP CH_4 concentrations are shown on the Greenland Ice Sheet Project 2 time scale from (*25*). The time scale of P09-PH2 is given on its own age model (fig. S2). The Heinrich events are depicted by the vertical arrows, and age estimations are from (*4*, *7*). The numbers indicate Greenland interstadials and Antarctic AIM events.

The primary climatic control on rainfall δ^{18}O for tropical South America is the amount of precipitation (*13*). Consistent with the "amount effect" (*14*) and Rayleigh-type fractionation during rainout, a stronger SASM leads to lower δ^{18}O values in tropical South American rainfall (*15*). Similar correlations have been made for other parts of the tropical Andes, where local precipitation δ^{18}O is strongly anticorrelated to rainfall amount upstream in the Amazon Basin rather than at the study site (*16*, *17*). Rayleigh distillation and moisture recycling in the Amazon Basin (*18*) preserve the isotopic signal of the monsoon along the moisture path from eastern Amazonia up to the central Peruvian Andes (*15*). On interannual time scales, the SASM is influenced by sea surface temperatures (SSTs) in the Atlantic and Pacific Oceans (*19*) and on orbital time scales by changes in insolation (*20*, *21*). These studies demonstrate that rainfall δ^{18}O in the central Andes records changes in the intensity of large-scale continental atmospheric convection, with more negative rainfall δ^{18}O values being indicative of enhanced SASM activity and increased rainout.

Comparison of the millennial-scale variability in the Pacupahuain Cave record to the isotopic fluctuations from Greenland (Fig. 1) shows that all D/O cycles are also found in our record of SASM intensity, with the sole exception of D/O event 3, which for unknown reasons is not present. The identification of D/O events is based on comparison to the North Greenland Ice Core Project (NGRIP) oxygen isotope record, using the ice core age model of (*22*) (Fig. 1) and the MSD speleothem record from Hulu Cave, China, using its own precise chronology (fig. S4) (*4*, *11*). Abrupt increases in NGRIP $\delta^{18}O_{ice}$, which characterize the onset of the D/O events, are clearly associated with rapid increases in $\delta^{18}O_{calcite}$ for P09-PH2. The relationship between D/O events in the NGRIP record and our results demonstrates that warm events in Greenland correspond to intervals of decreased SASM intensity. The timing of millennial-scale variability is synchronous within the independent age model errors.

Figure 1 also includes the record of atmospheric methane (CH_4) concentrations from Greenland and Antarctic ice cores (*23*–*25*). The origin

of millennial-scale variations in atmospheric CH_4 is not certain, although they are thought to arise from changes in the flux from global wetlands (*26*, *27*) rather than from the release of CH_4 from marine clathrates (*28*) or changes in CH_4 removal via oxidation in the troposphere (*26*). Whether source flux changes derive from tropical wetlands or boreal forests has not been established. We observe that increases in global atmospheric CH_4 occur contemporaneously with increases in P09-PH2 $\delta^{18}O$ and reduced SASM intensity (Fig. 1). Thus, the Southern Hemisphere South American tropics are unlikely to be a source of increased atmospheric CH_4, via wetland expansion, during Greenland interstadials. The interhemispheric antiphasing of the tropical monsoon systems during D/O events, however, indicates that rapid northward shifts of the Intertropical Convergence Zone (ITCZ) and intensification of the EASM and ISM might lead to wetland expansion and increased CH_4 production in the Northern Hemisphere tropics during warm Greenland intervals.

In addition to the millennial-scale D/O events, each Heinrich event (H1 through H5) can also be identified in the P09-PH2 reconstruction by periods of enhanced SASM activity (Fig. 1) and by correlation to decreased Asian monsoon intensity based on the Hulu Cave record (fig. S4) (*4*, *11*). Previous paleoclimate studies of the SASM, which reconstructed precipitation intensity during the Last Glacial period but at lower resolution than presented here, also identified Heinrich events as particularly wet intervals (*29*, *30*). Increased Heinrich event precipitation over tropical South America is supported by evidence of substantial lateral advancement of central Andean glaciers during H1 and H2 (*31*) and increases in precipitation over northeast Brazil for H1 through H5 (*30*, *32*, *33*).

The expression of D/O cycles and Heinrich events in SASM variability is antiphased with Northern Hemisphere monsoon precipitation reconstructions over the Last Glacial period. Our record indicates a weak SASM during D/O interstadials, but reconstructions of Indian Ocean climate (*2*) and EASM intensity (*4*) demonstrate very wet intervals for interstadial phases. Although previous work has demonstrated such antiphase behavior for orbital-scale climate variability in the tropics (*21*) and for Heinrich events (*30*), it had not been unequivocally determined for D/O scale variability. Such antiphase behavior can be explained by latitudinal shifts of the ITCZ driven by rapid Northern Hemisphere temperature fluctuations. Modeling data demonstrate ITCZ migration away from the hemisphere with high-latitude cooling and added ice cover (*34*). During pronounced North Atlantic cold events, southward migration of the ITCZ can alter Hadley cell circulation, increase subsidence (dry conditions) for the northern branch, and intensify uplift (wet conditions) of the southern branch (*35*, *36*). As a result, the ISM and EASM weaken and the SASM intensifies. Although our record is short relative to precessional-scale insolation changes, insolation appears to be only weakly expressed in our record (fig. S5).

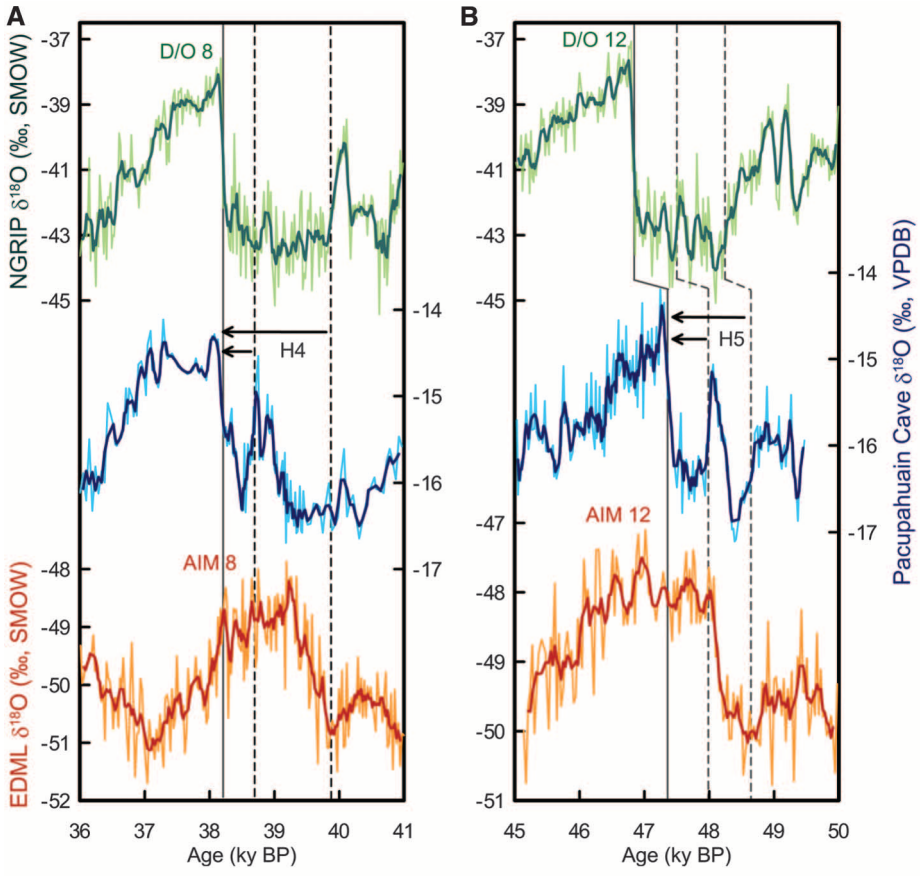

Fig. 2. Detailed view of the $\delta^{18}O$ records from Pacupahuain Cave (blue) and Greenland (green) and Antarctic (red) ice cores during (**A**) Heinrich event 4 and D/O and AIM events 8 and (**B**) Heinrich event 5 and D/O and AIM events 12. The solid black vertical line indicates the end of Heinrich events H4 and H5, and the dashed black vertical lines indicate two possible onsets for Heinrich events H4 and H5. Isotope records and corresponding age models are the same as in Fig. 1.

In addition to demonstrating the presence of D/O and Heinrich variability in the SASM, our record reveals additional rapid, millennial-scale climate reversals in the tropical climate record. These events appear to arise from the interplay between Northern and Southern Hemisphere high-latitude climate change. The reversals are most clearly expressed at 38.75 and 48 ky B.P. during extended Greenland stadials (Fig. 2). We propose that the onset of these events coincides with the onset of Antarctic Isotope Maxima (AIM) events 8 and 12 in the EPICA (European Project for Ice Coring in Antarctica) Dronning Maud Land (EDML) ice core record (*22*). Prolonged Greenland cold phases have been linked with intensification and southward displacement of the Southern Hemisphere westerlies, enhanced upwelling in the Southern Ocean, rising atmospheric CO_2, and Antarctic warming (*37*, *38*). Specifically, the opal flux reconstruction presented in (*38*) demonstrates that ocean upwelling and CO_2 rises were largest during H4 and H5 as compared to more recent Heinrich events. Thus, we propose that enhanced changes in Southern Ocean climate specific to H4 and H5 can explain why our record shows reversals in SASM vigor at H4 and H5 and not for the later Heinrich events.

The precise relation between these transient millennial-scale events and the ice-rafted components of Heinrich events H4 and H5, which occurred at approximately the same time period, is less clear. It is well established that the endings of H4 and H5 occur with Greenland warming at D/O events 8 and 12, respectively, but the beginnings of H4 and H5 are less well constrained. One interpretation based on our record is that the onset of Heinrich events H4 and H5 began with the sharp increase in SASM intensity that follows the decrease associated with Antarctic warming. An abrupt increase in SASM intensity associated with Heinrich events has been recognized in marine (*32*, *33*) and terrestrial (*29*, *30*) records. This sequence of events would restrict the duration of H4 and H5 events to <400 years, which has previously been suggested for H4 (*39*). It would also indicate that Antarctic warming precedes the start of Heinrich events 4 and 5. Antarctic warming has previously been proposed as a trigger for H1 (*40*). A second possibility,

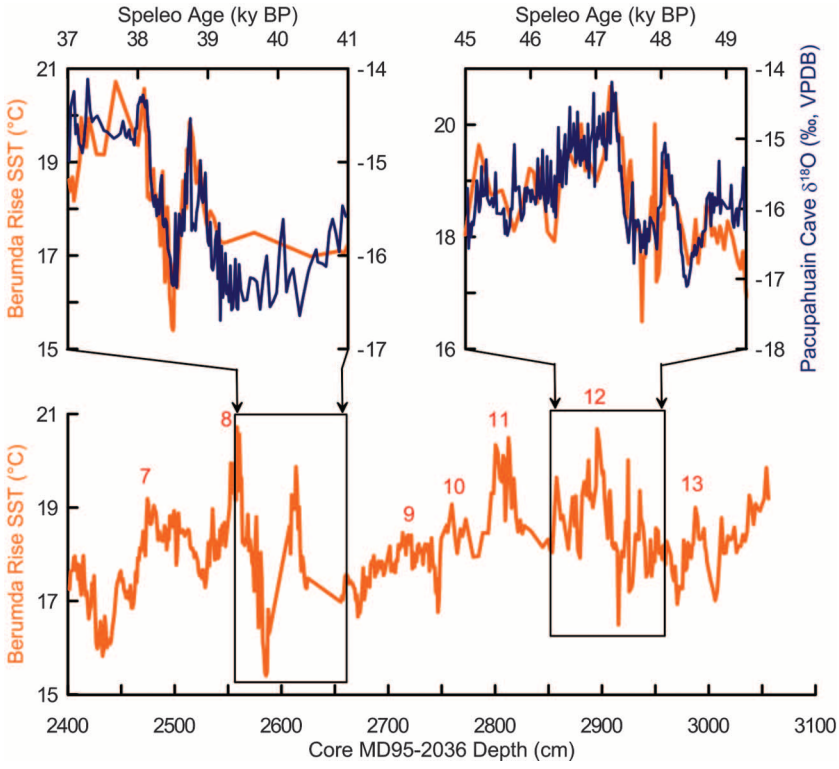

Fig. 3. Bermuda Rise SSTs (orange) shown to depth in core MD95-2036 (*41*). D/O events were identified on the basis of visual correlation to the Greenland isotope temperature record as in (*41*). An expanded view of results from our P09-PH2 record (blue) and subtropical Atlantic SSTs (orange) using our revised age model (*11*) is shown for the intervals of H4 (left) and H5 (right).

however, is that H4 and H5 may have begun before the weakening of the SASM and Antarctic warming and thus lasted throughout the extended Greenland cold phase. Although in this case we have no explanation for why the SASM suddenly strengthened.

One final aspect of the SASM reversals before D/O events 8 and 12 is unusual. High northern latitude warming is associated with an intensification of the Northern Hemisphere monsoons. By analogy, high southern latitude warming might be expected to result in intensification of the SASM, but the opposite is observed. This seeming contradiction can be reconciled by comparison of our record to a high-resolution SST record based on alkenone paleothermometry from the Bermuda Rise (33.69°N, 57.56°W) (*41*). Core MD95-2036 shows large, rapid, warm intervals (warmer by 3° to 5°C) immediately before D/O events 8 and 12, which were originally interpreted as instabilities during the rapid transitions of the largest Greenland interstadials. Based on visual comparison, we establish tie points between the Bermuda Rise SST record and our $\delta^{18}O$ record and provide a revised age model for these two oscillations in Bermuda Rise SSTs (*11*) (Fig. 3). The original marine core chronology was based on maximizing the correlation to the Greenland ice core record and its chronology at the time of publication (*11*, *42*). Our revised chronology for the two intervals of MD95-2036 places the warm intervals 600 ± 100 years earlier, relative to an updated Greenland chronology, which is well within the thousand-year uncertainty of the original marine core age model. Thus, Antarctic warming at AIM events 8 and 12 may be associated with a weakened SASM as described above (Fig. 2), as well as a warmer subtropical North Atlantic Ocean (Fig. 3) (*41*). Similar temperature reversals within H4 and H5 have been identified in a deep water record from the Iberian Margin (*43*). It is not clear why Antarctic warming is associated with warming in the subtropical North Atlantic, although one result of the latter could be a northward shift of the ITCZ in the Atlantic Ocean sector (*44*) due to a weakening of the subtropical Atlantic gyre. The association between warm SSTs in the Bermuda Rise region, a weakening of the SASM, and a more northerly position of the ITCZ, as we have described for the D/O events, could also be applied to the additional reversals identified in Fig. 3.

References and Notes

1. W. Dansgaard *et al.*, *Nature* **364**, 218 (1993).
2. S. J. Burns, D. Fleitmann, A. Matter, J. Kramers, A. A. Al-Subbary, *Science* **301**, 1365 (2003).
3. Y. Wang *et al.*, *Nature* **451**, 1090 (2008).
4. Y. J. Wang *et al.*, *Science* **294**, 2345 (2001).
5. H. Heinrich, *Quat. Res.* **29**, 142 (1988).
6. G. Bond *et al.*, *Nature* **360**, 245 (1992).
7. S. R. Hemming, *Rev. Geophys.* **42**, RG1005 (2004).
8. T. F. Stocker, *Radiocarbon* **40**, 359 (1998).
9. E. J. Cobbing *et al.*, in *The Geology of the Western Cordillera of Northern Peru* (Great Britian Institute of Geological Sciences, Natural Environment Research Council, London, 1981), p. 143.
10. H. Cheng *et al.*, *Geology* **37**, 1007 (2009).
11. Information on materials and methods is available as supporting material on *Science* Online.
12. C. H. Hendy, *Geochim. Cosmochim. Acta* **35**, 801 (1971).
13. M. Vuille, R. S. Bradley, M. Werner, R. Healy, F. Keimig, *J. Geophys. Res.* **108**, 4174 (2003).
14. W. Dansgaard, *Tellus* **16**, 436 (1964).
15. M. Vuille, M. Werner, *Clim. Dyn.* **25**, 401 (2005).
16. F. Vimeux, R. Gallaire, S. Bony, G. Hoffmann, J. Chiang, *Earth Planet. Sci. Lett.* **240**, 205 (2005).
17. G. Hoffmann *et al.*, *Geophys. Res. Lett.* **30**, 1179 (2003).
18. R. L. Victoria, L. A. Martinelli, J. Mortatti, J. Richey, *Ambio* **20**, 384 (1991).
19. M. Vuille, R. S. Bradley, F. Keimig, *J. Geophys. Res.* **105**, 12447 (2000).
20. G. Seltzer, D. Rodbell, S. Burns, *Geology* **28**, 35 (2000).
21. F. W. Cruz Jr. *et al.*, *Nature* **434**, 63 (2005).
22. B. Lemieux-Dudon *et al.*, *Quat. Sci. Rev.* **29**, 8 (2010).
23. C. Barbante *et al.*; EPICA Community Members, *Nature* **444**, 195 (2006).
24. J. Flückiger, *Global Biogeochem. Cycles* **18**, GB1020 (2004).
25. T. Blunier, E. J. Brook, *Science* **291**, 109 (2001).
26. J. Chappellaz *et al.*, *Nature* **366**, 443 (1993).
27. A. Dällenbach *et al.*, *Geophys. Res. Lett.* **27**, 1005 (2000).
28. M. Bock *et al.*, *Science* **328**, 1686 (2010).
29. X. Wang *et al.*, *Quat. Sci. Rev.* **25**, 3391 (2006).
30. X. F. Wang *et al.*, *Nature* **432**, 740 (2004).
31. J. A. Smith, D. T. Rodbell, *J. Quat. Sci.* **25**, 243 (2010).
32. A. Jaeschke, C. Ruhlemann, H. Arz, G. Heil, G. Lohmann, *Paleoceanography* **22**, PA4206 (2007).
33. T. C. Jennerjahn *et al.*, *Science* **306**, 2236 (2004).
34. J. C. H. Chiang, C. M. Bitz, *Clim. Dyn.* **25**, 477 (2005).
35. R. Zhang, T. L. Delworth, *J. Clim.* **18**, 1853 (2005).
36. A. C. Clement, L. C. Peterson, *Rev. Geophys.* **46**, RG4002 (2008).
37. G. H. Denton *et al.*, *Science* **328**, 1652 (2010).
38. R. F. Anderson *et al.*, *Science* **323**, 1443 (2009).
39. D. Roche, D. Paillard, E. Cortijo, *Nature* **432**, 379 (2004).
40. A. J. Weaver, O. A. Saenko, P. U. Clark, J. X. Mitrovica, *Science* **299**, 1709 (2003).
41. J. P. Sachs, S. J. Lehman, *Science* **286**, 756 (1999).
42. E. A. Boyle, *Proc. Natl. Acad. Sci. U.S.A.* **94**, 8300 (1997).
43. L. C. Skinner, H. Elderfield, *Paleoceanography* **22**, PA1205 (2007).
44. A. J. Broccoli, K. A. Dahl, R. J. Stouffer, *Geophys. Res. Lett.* **33**, L01702 (2006).

Acknowledgments: This work is supported by NSF grant ATM-1003466 to S.J.B., NSF grants 0502535 and 1103403 to R.L.E. and H.C., and Geological Society of America Student Award 9308-10 to L.C.K. We thank C. Morales-Bermudez for his invaluable assistance in the field. Comments from two anonymous reviewers substantially improved the manuscript. The data in this paper are tabulated in the supporting online material and are archived online at ftp://ftp.ncdc.noaa.gov/pub/data/paleo.

Supporting Online Material

www.sciencemag.org/cgi/content/full/science.1213397/DC1
Materials and Methods
Figs. S1 to S5
Table S1
References (*45*–*51*)

31 August 2011; accepted 4 January 2012
Published online 12 January 2012;
10.1126/science.1213397